The influence of hemispheric asymmetries on field-aligned ion drifts at the geomagnetic equator

A. G. Burrell[1,2] and R. A. Heelis[2]

Received 20 August 2012; accepted 30 August 2012; published 4 October 2012.

[1] In the topside ionosphere, equatorial field-aligned ion drifts are driven by field-aligned gradients in the plasma pressure. These gradients form due to hemispheric asymmetries in plasma temperature and density, which are caused by the sun and the neutral atmosphere. The role of the neutral atmosphere in creating a field-aligned plasma pressure gradient and driving ion drifts across the geomagnetic equator is examined for several local times during solar minimum. Using satellite observations and complimentary modeled data, the field-aligned ion drifts are found to correlate with the vertical displacement between conjugate ion density peaks in both the observed and modeled data sets. In the modeled data sets, an even stronger correlation is seen between the field-aligned ion drift and the total neutral wind along the magnetic meridian at the height of the ion density peak. This correlation is seen to improve in the absence of an $\mathbf{E} \times \mathbf{B}$ drift. **Citation:** Burrell, A. G., and R. A. Heelis (2012), The influence of hemispheric asymmetries on field-aligned ion drifts at the geomagnetic equator, *Geophys. Res. Lett.*, *39*, L19101, doi:10.1029/2012GL053637.

1. Introduction

[2] In the topside ionosphere, field-aligned ion drifts are produced by latitudinal gradients in the plasma pressure along the magnetic field. The presence of field-aligned ion drifts can most easily be inferred from observations of the latitude profile of plasma density [*West et al.*, 1997], though their presence can also be inferred from plasma temperature gradients caused by the adiabatic expansion and compression of the ionosphere as plasma moves parallel to the magnetic field [*Venkatraman and Heelis*, 2000]. While ionospheric models have been used to infer the magnitude of interhemispheric transport that would be required to reproduce a given distribution of the plasma temperatures [*Bailey and Heelis*, 1980], only recently has a comprehensive description of the field-aligned ion drifts been published [*Burrell et al.*, 2011, 2012]. This description clearly demonstrates the contributions of hemispheric asymmetries in the field-aligned plasma density to the field-aligned ion drifts.

[3] Sources of field-aligned plasma density asymmetries include hemispheric asymmetries in ion production and loss rates as well as in the lower thermospheric neutral wind along the magnetic meridian. The lower thermospheric neutral wind modulates the field-aligned ion drifts by altering the height of the F peak (h_mF_2), which changes the topside volume available to the plasma and alters the effective loss rate of the plasma. *Burrell et al.* [2012] used data from the Coupled Ion Neutral Dynamics Investigation (CINDI) and the Formosa Satellite-3/Constellation Observing System for Meteorology, Ionosphere, and Climate (F3/C) GPS Occultation eXperiment (GOX) to show that, apart from sunrise and sunset when rapid net ion production and loss occur, the behavior of the topside field-aligned ion drifts is associated with neutral wind driven latitudinal asymmetries in the h_mF_2 observed by GOX. This relationship motivates a more rigorous investigation into the dependence of the field-aligned ion drifts on forcing from the lower thermospheric neutral wind, which produces the hemispheric asymmetry in the h_mF_2. In this paper these same data sets are used to quantify the relationship between the field-aligned ion drifts in the topside equatorial ionosphere and the hemispheric asymmetry in the h_mF_2. Additionally, Sami2 is Another Model of the Ionosphere (SAMI2) and the Horizontal Wind Model (HWM) are used to gain more insight into the processes at work.

2. Data

[4] Observations for this investigation were gathered during solar minimum from the CINDI sensors onboard the Communication/Navigation Outage Forecasting System (C/NOFS) satellite [*de la Beaujardière*, 2004]. The C/NOFS satellite was launched on 16 April, 2008 into an equatorial, low earth orbit with an inclination of 13° and an orbital period of about 97 min. Two instruments from the CINDI mission were used to obtain the three-dimensional ion velocity: the retarding potential analyzer and the ion drift meter [*Heelis and Hanson*, 1998]. The field-aligned component of the ion velocity, $v_{\|}$, was then obtained using the International Geomagnetic Reference Field (IGRF) [*Maus et al.*, 2005].

[5] Measurements of the height of the ion density peak, h_mF_2, were taken from electron density profiles obtained from the GOX instrument, which flies onboard each of the six microsatellites that make up the F3/C constellation. *Yue et al.* [2010] showed that the F3/C h_mF_2 error was approximately 7.4 km globally. To exclude any instances where the altitude of the peak electron density cannot physically represent the h_mF_2, only peak altitudes greater than 120 km were used.

[6] To ensure a high data quality, this study used observations taken between 14 November, 2008 and 20 October,

[1]Atmospheric, Oceanic, and Space Sciences, University of Michigan, Ann Arbor, Michigan, USA.
[2]William B. Hanson Center for Space Sciences, University of Texas at Dallas, Richardson, Texas, USA.

Corresponding author: A. G. Burrell, Atmospheric, Oceanic, and Space Sciences, University of Michigan, 2455 Hayward St., Ann Arbor, MI 48109, USA. (agburr@umich.edu)

0094-8276/12/2012GL053637

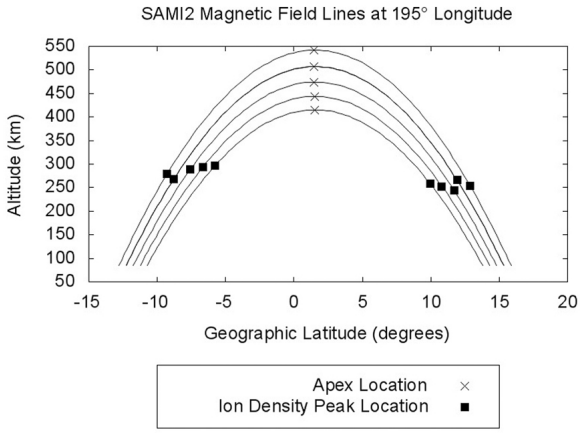

Figure 1. Pairing apex field-aligned drifts and northern and southern h_mF_2 locations for SAMI2 field lines.

2009 on days with Kp ≤ 3. Three seasons of four months each, centered about the solstice and equinox dates, were used to ensure complete data coverage, even though this method assumes that there is little difference between the March and September equinox behaviors. Four local time sectors were used to constrain the contribution from local time dependence, covering the morning (07:30–10:30), daytime (10:30–15:00), evening (17:30–21:30), and nighttime (23:00–03:00) hours. The CINDI data were restricted to altitudes between 400–550 km and corrected geomagnetic latitudes within 5° of the geomagnetic equator. The F3/C h_mF_2 were restricted to geographic latitudes within 5° of the northern and southern flux tube feet. The flux tube feet locations were computed every 5° longitude using dipole field equations with an apex height given by the median apex height of the CINDI observations and a foot height of 250 km. Running medians of CINDI field-aligned ion drifts and the F3/C conjugate h_mF_2 displacement (found by subtracting the southern h_mF_2 from the northern h_mF_2) were then computed at these locations. *Burrell et al.* [2012] described this data set in more detail.

[7] Modeled data sets were obtained using SAMI2-1.00 [*Huba et al.*, 2000] (altered to use the 2007 version of HWM [*Drob et al.*, 2008]), which provides the field-aligned drift, temperature, and density for seven ion species. Two model runs were performed, one using the standard $\mathbf{E} \times \mathbf{B}$ drift [*Scherliess and Fejer*, 1999] and the other using no $\mathbf{E} \times \mathbf{B}$ drift. Both runs were performed at a weekly cadence for the year covered by the CINDI and F3/C observations at 35 evenly spaced longitudes starting at 5° longitude. The model was run using 30 magnetic field lines with apex heights between 150 and 1,500 km, though data was only taken from those that peaked between 400 and 550 km. In order to match the CINDI and F3/C observations as closely as possible, the field-aligned O^+ drift, $v_{O_{||}^+}$, at the field line apex was paired with the northern and southern h_mF_2 along the same field line when the O^+ concentration at the apex was over 90% of the total. This pairing is illustrated in Figure 1. The h_mF_2 were computed by finding the location of the maximum total ion density every 1° of latitude at each longitude and timestep. Finally, HWM was run at every northern and southern h_mF_2 and the component along the magnetic meridian, $u_{||}$, was computed using IGRF. The seasonal and local time medians of the field-aligned O^+ drift, conjugate h_mF_2 displacement, and conjugate $u_{||}$ sum (the sum of the neutral wind along the magnetic meridian at the northern and southern h_mF_2) were then computed at each longitude.

3. Results and Discussion

[8] Figure 2 shows the field-aligned ion drift plotted versus the conjugate h_mF_2 displacement, along with the best-fit line for the four local time regions described earlier. Positive (negative) field-aligned ion drifts are directed to the north (south) and positive (negative) conjugate h_mF_2 displacements lead to field-aligned plasma pressure gradients that drive northbound (southbound) field-aligned ion drifts.

[9] In the topside ionosphere the ion-neutral collision frequency is very low, and at the geomagnetic equator the gravitational force is directed perpendicular to the magnetic field. Thus, the field-aligned ion drift will only depend on the field-aligned plasma pressure gradient. If the field-aligned changes in the plasma temperature are small, then this dependence will reduce to a dependence on the field-aligned plasma density gradient.

[10] The field-aligned plasma density gradient depends on the conjugate differences in the h_mF_2 and N_mF_2, or the peak ion density. As the h_mF_2 specifies the plasma loss rate at that location, the N_mF_2 is itself related to the peak height. Thus, a strong linear dependence between the field-aligned ion drift and the conjugate h_mF_2 displacement emerges. Non-zero intercepts and scatter about the best-fit line suggest the presence of other processes or conditions that decouple the dependence of the N_mF_2 on h_mF_2.

[11] The morning region, shown in Figure 2a, has the most significant offset in the intercept. The value clearly cannot be attributed to the influence of the scatter on the linear regression. At these local times the recent onset of photoionization has not subsided at all longitudes and field-aligned plasma temperature gradients are also significant [*Oyama et al.*, 1996]. The continued existence of a linear relationship between the field-aligned ion drift and the conjugate h_mF_2 displacement shows that the h_mF_2 is responding to the production of ionization as well as the neutral wind. The large intercept in this relationship suggests that field-aligned ion drifts also result from a constant hemispheric asymmetry in the net ionization production rate.

[12] At the local times shown in Figures 2b–2d, the non-Gaussian distributions of the scatter about the best-fit line are more pronounced than the small, non-zero intercepts. One such instance is shown in Figure 2b, where a significant field-aligned drift appears for several points when the conjugate h_mF_2 displacement is small. These deviations from the best-fit line lead to a skew of −1.112, which indicates an asymmetrical distribution that favors values lower than those on the best-fit line. A large skew or weaker R^2 value both indicate the presence of other important physical processes that may produce hemispheric asymmetries in the topside ionosphere without changing the h_mF_2. One such physical process is the meridional $\mathbf{E} \times \mathbf{B}$ drift. Because it is difficult to decouple the influences of lower thermospheric neutral winds and the $\mathbf{E} \times \mathbf{B}$ drift in the data, these influences are explored in more detail using SAMI2.

[13] Figure 3 presents the SAMI2 equivalent of Figure 2; Figures 3a–3d show the field-aligned O^+ drift versus the conjugate h_mF_2 displacement from the SAMI2 run with the

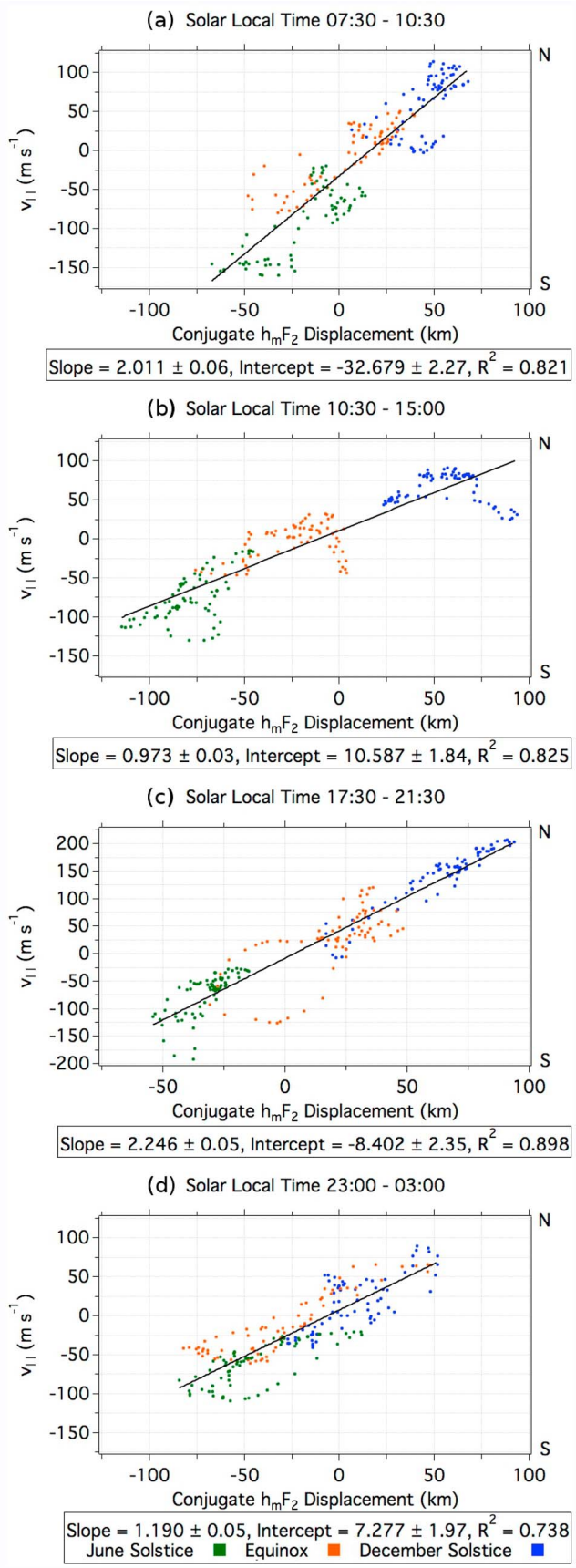

Figure 2. Correlation between the CINDI field-aligned drift and the F3/C conjugate h_mF_2 displacement within 5° of the geomagnetic equator at four solar local time bins.

standard **E** × **B** drift and Figures 3e–3h show the equivalent plots using data from the SAMI2 run with no **E** × **B** drift. The degree of similarity between the plots in this figure and those in Figure 2 is remarkable. The seasonal variations in the field-aligned ion drift and conjugate h_mF_2 displacement are the same and the slopes of the best-fit lines share similar variations in local time. The largest slopes are seen in the morning and at dusk (Figures 3a, 3c, 3d, and 3e), while the smallest slopes are seen during the day and at night (Figures 3b, 3d, 3f, and 3h).

[14] The differences in the linear trends between the two SAMI2 runs reveal the influence of the meridional **E** × **B** drift on the field-aligned ion drift. An upward meridional **E** × **B** drift transports the plasma to higher altitudes on larger magnetic flux tubes, increasing the available volume and thereby decreasing any existing field-aligned plasma pressure gradient. A downward meridional **E** × **B** drift does the opposite, increasing any existing field-aligned plasma pressure gradient. At night the **E** × **B** drift model generally shows a downward meridional **E** × **B** drift, which would increase any field-aligned drifts at the geomagnetic equator caused by conjugate h_mF_2 displacements. A comparison of Figures 3d and 3h confirms this by noting that the slope has decreased in the SAMI2 run without any **E** × **B** drift. Likewise, in the morning the **E** × **B** drift model shows that an upward meridional **E** × **B** drift is present. As this meridional **E** × **B** drift would reduce any existing field-aligned ion drifts, the slope of the best-fit line in Figure 3a should be (and is) smaller than that shown in Figure 3d. Thus local time variations in the magnitude of the best-fit line slope must include contributions from the meridional **E** × **B** drift. Differences between the linear trends fit to the observations in Figure 2 and the modeled data in Figure 3 can be attributed to documented differences between these measured and modeled quantities [*Stoneback et al.*, 2011; *Emmert et al.*, 2010]. Comparing the R^2 values in Figures 3c and 3g suggests that the meridional **E** × **B** drift plays an important role in altering the field-aligned drift in the evening. This is not the case at all local times, though, as can be seen by examining the R^2 values for the nighttime period shown in Figures 3d and 3h. Here, ion loss processes likely have a greater affect on the field-aligned drift than the meridional **E** × **B** drift.

[15] The component of the neutral wind along the magnetic meridian and the meridional **E** × **B** drift have been shown to be among the primary reasons for changes in the h_mF_2 [*Rishbeth*, 1967; *Luan and Solomon*, 2008; *Miller et al.*, 1986]. Figure 4, which follows the same format as Figure 3, explores the relationship between the lower thermospheric neutral wind and the conjugate h_mF_2 displacement by replacing the field-aligned ion drift on the y-axis with the conjugate $u_{||}$ sum. A positive linear relationship exists between the conjugate $u_{||}$ sum and the conjugate h_mF_2 displacement. This relationship is in agreement with the established connection between the neutral wind and the h_mF_2, and is stronger when the meridional **E** × **B** drift is not affecting the F_2 peak characteristics.

[16] As the neutral wind has been successfully tied to the conjugate h_mF_2 displacement, it is then reasonable to ask to what extent the conjugate $u_{||}$ sum may be related to the interhemispheric transport of ions. Figure 5 explores this possibility, plotting the field-aligned O^+ drift versus the conjugate $u_{||}$ sum using the same format as Figures 3 and 4.

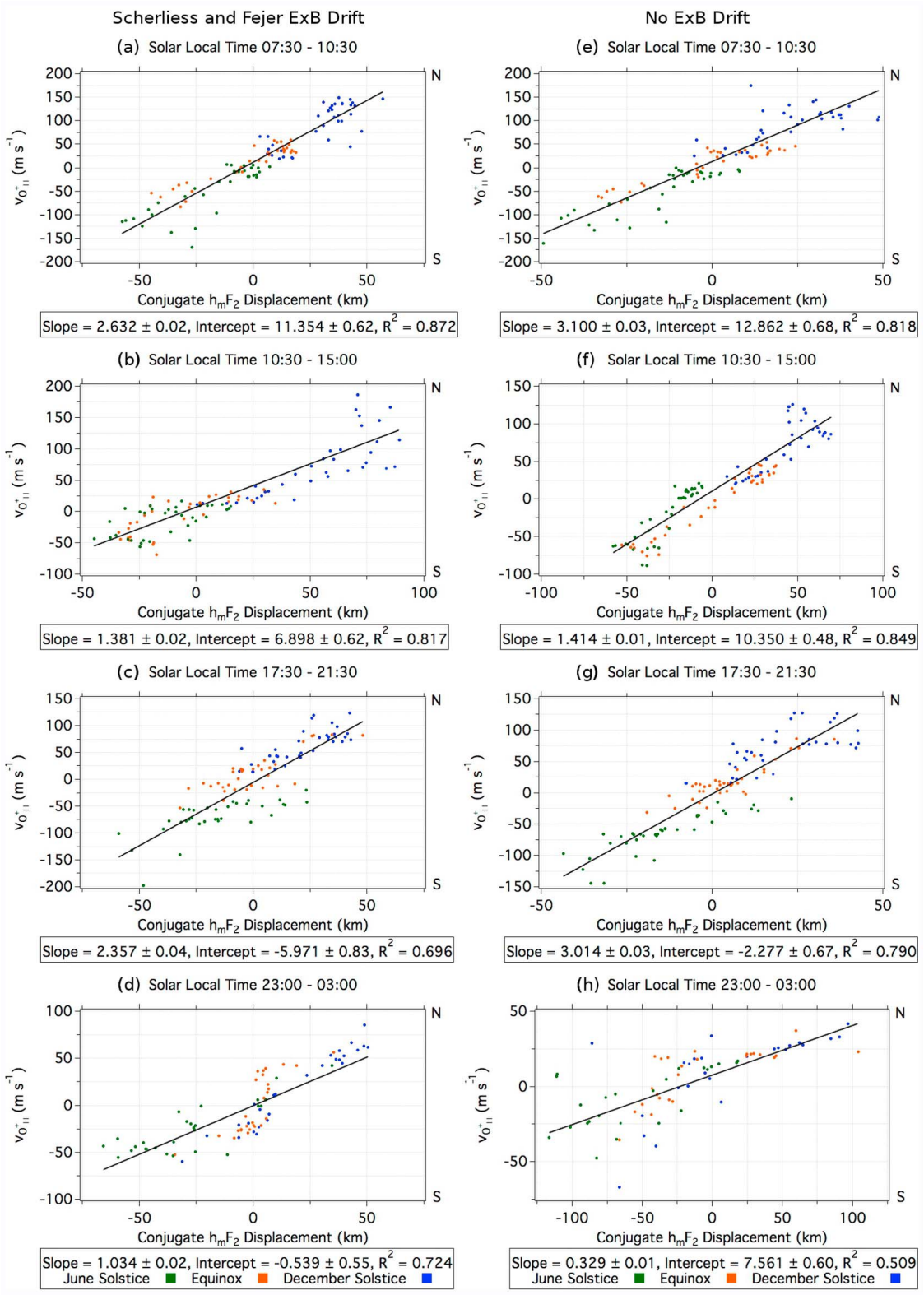

Figure 3. Correlation between the SAMI2 field-aligned drift and conjugate h_mF_2 displacement within 5° of the geomagnetic equator at four solar local time bins. (a–d) The runs that used Fejer-Scherliess **E** × **B** drifts, and (e–h) those that were run without **E** × **B** drifts.

The linear correlation follows the same daily changes in slope seen between the field-aligned drift and conjugate h_mF_2 displacement. As expected, given the differences between the SAMI2 runs with and without **E** × **B** drift, the correlation is stronger in the SAMI2 run without **E** × **B** drift. Comparing Figures 3e–3h and Figure 5e–5h reveals that the R^2 of the best-fit line relating the field-aligned drift to the conjugate $u_{||}$ sum is higher than the R^2 for the best-fit line

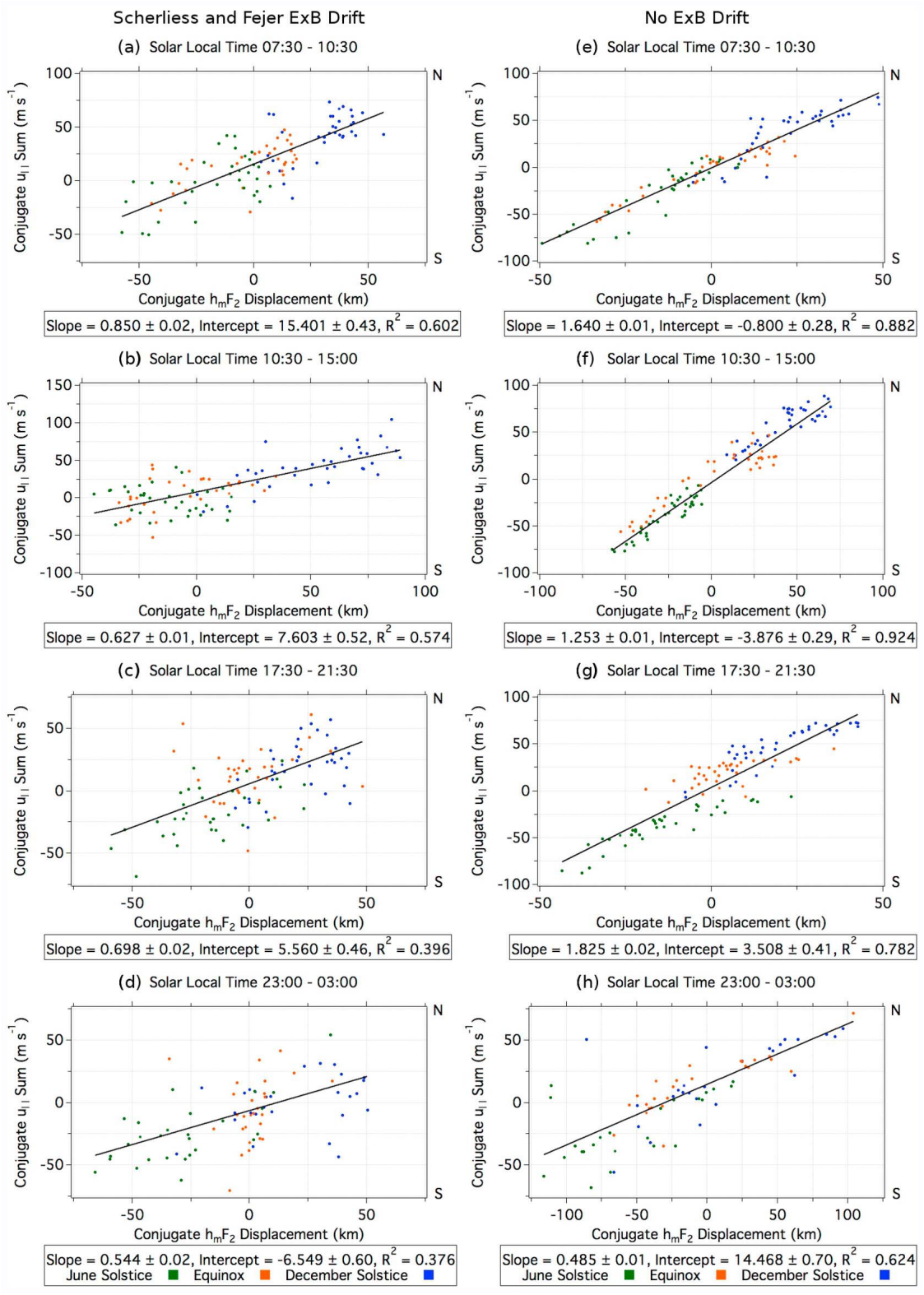

Figure 4. Correlation between the HWM conjugate neutral wind sum and the SAMI2 conjugate h_mF_2 displacement within 5° of the geomagnetic equator at four solar local time bins. (a–d) The runs that used Fejer-Scherliess $\mathbf{E} \times \mathbf{B}$ drifts, and (e–h) those that were run without $\mathbf{E} \times \mathbf{B}$ drifts.

relating the field-aligned drift to the conjugate h_mF_2 displacement at all local times except during the day (Figure 3f), where it is equally good in both cases. This suggests that the conjugate $u_{||}$ sum more faithfully captures the combination of differences in the conjugate h_mF_2 and N_mF_2 than the conjugate h_mF_2 displacement alone.

[17] At local times where the assumption of quasi-steady state holds, the relationship between the field-aligned ion

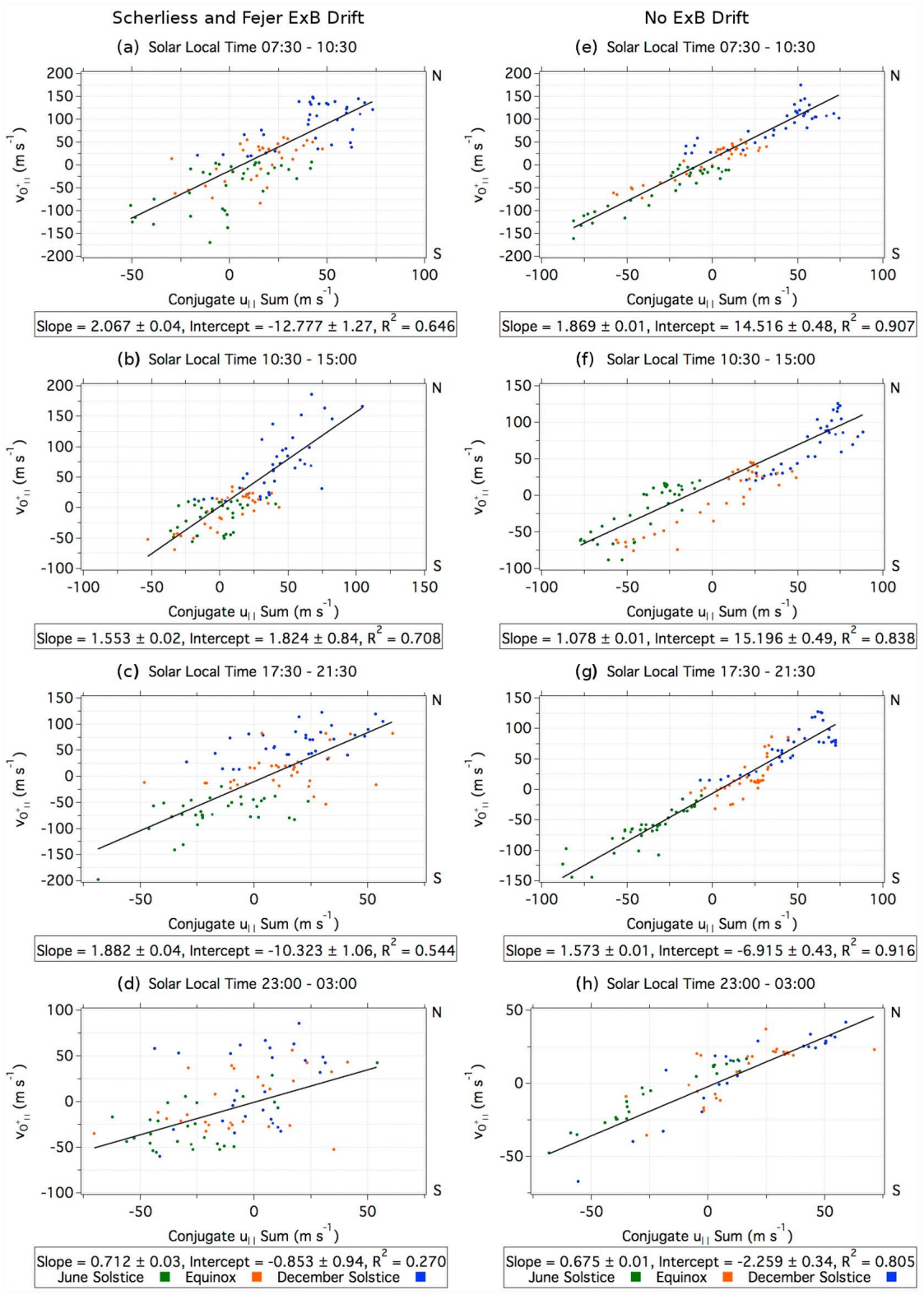

Figure 5. Correlation between the SAMI2 field-aligned drift and the HWM conjugate neutral wind sum within 5° of the geomagnetic equator at four solar local time bins. (a–d) The runs that used Fejer-Scherliess **E** × **B** drifts, and (e–h) those that were run without **E** × **B** drifts.

drift and the conjugate $u_{||}$ sum indicates that the field-aligned ion drift can be used to obtain an estimate of the conjugate $u_{||}$ sum, similar to the proxy computed by *Sultan and Rich* [2001]. The conjugate h_mF_2 displacement may also be used to obtain an estimate of the conjugate $u_{||}$ sum (or field-aligned ion drift), similar to those computed by *Rishbeth* [1967], *Miller et al.* [1986], and *Luan and Solomon* [2008]. These authors, however, used both the h_mF_2 and

the N_mF_2 to estimate the neutral wind along the magnetic meridian. The direct inclusion of the N_mF_2 has not been included in this study, but given the typical decrease in the R^2 values between Figures 3e–3h and 5e–5h, its inclusion in a field-aligned plasma pressure gradient proxy should reduce the scatter about the best-fit lines.

4. Conclusions

[18] A linear relationship between the difference in the conjugate h_mF_2 on a given magnetic flux tube and the field-aligned ion drifts at the apex of that flux tube has been clearly established in observations and shown to be a natural outcome in the output of the SAMI2 ionospheric model. While typically only 80% of the variation in the field-aligned drifts may be attributed to the conjugate h_mF_2 displacement, the correlation is notable because the field-aligned ion drifts are dependent on the local field-aligned plasma pressure gradient. When the assumption of quasi-steady state holds, the field-aligned ion drift at the geomagnetic equator will be proportional to the density difference at a fixed height above the ion density peak. This difference will depend on the both the N_mF_2 and the h_mF_2, though the N_mF_2 is itself related to the h_mF_2. Therefore, a strong correlation exists between the field-aligned ion drift and the conjugate h_mF_2 displacement alone. In the absence of a meridional $\mathbf{E} \times \mathbf{B}$ drift, the strong correlation between the conjugate $u_{\|}$ sum and the field-aligned drift introduces the possibility of creating a proxy for this characteristic of the F-region neutral wind. Although it was impossible to validate the SAMI2 correlation between the field-aligned drift and the conjugate $u_{\|}$ sum with data due to the lack of neutral wind observations, future missions that include a measurement of the lower thermosphere neutral wind should be able to directly test the correlation between the winds and the field-aligned drifts at the equator.

[19] **Acknowledgments.** This work was supported by NASA grants NAS5-01068 and NNX10AT02G. The authors would like to thank the F3/C orbital operation team at the National Space Organization (supported by the National Science Council of Taiwan) and the University Corporation for Atmospheric Research for their roles in obtaining and distributing the F3/C data. The Editor thanks two anonymous reviewers for assisting in the evaluation of this paper.

References

Bailey, G. J., and R. A. Heelis (1980), Ion temperature troughs induced by a meridional neutral air wind in the night-time equatorial topside ionosphere, *Planet. Space Sci.*, *28*(9), 895–906, doi:10.1016/0032-0633(80)90062-8.

Burrell, A. G., R. A. Heelis, and R. A. Stoneback (2011), Latitude and local time variations of topside magnetic field-aligned ion drifts at solar minimum, *J. Geophys. Res.*, *116*, A11312, doi:10.1029/2011JA016715.

Burrell, A. G., R. A. Heelis, and R. A. Stoneback (2012), Equatorial longitude and local time variations of topside magnetic field-aligned ion drifts at solar minimum, *J. Geophys. Res.*, *117*, A04304, doi:10.1029/2011JA017264.

de la Beaujardière, O. (2004), C/NOFS: A mission to forecast scintillations, *J. Atmos. Sol. Terr. Phys.*, *66*(17), 1573–1591.

Drob, D. P., et al. (2008), An empirical model of the Earth's horizontal wind fields: HWM07, *J. Geophys. Res.*, *113*, A12304, doi:10.1029/2008JA013668.

Emmert, J. T., J. L. Lean, and J. M. Picone (2010), Record-low thermospheric density during the 2008 solar minimum, *Geophys. Res. Lett.*, *37*, L12102, doi:10.1029/2010GL043671.

Heelis, R. A., and W. B. Hanson (1998), Measurements of thermal ion drift velocity and temperature using planar sensors, in *Measurement Techniques in Space Plasmas: Particles*, *Geophys. Monogr. Ser.*, vol. 102, edited by F. Pfaff, E. Borovsky, and T. Young, pp. 61–71, AGU, Washington, D. C.

Huba, J. D., G. Joyce, and J. A. Fedder (2000), Sami2 is Another Model of the Ionosphere (SAMI2): A new low-latitude ionosphere model, *J. Geophys. Res.*, *105*(A10), 23,035–23,053.

Luan, X., and S. C. Solomon (2008), Meridional winds derived from COSMIC radio occultation measurements, *J. Geophys. Res.*, *113*, A08302, doi:10.1029/2008JA013089.

Maus, S., et al. (2005), The 10th generation international geomagnetic reference field, *Phys. Earth Planet. Inter.*, *151*(3–4), 320–322, doi:10.1016/j.pepi.2005.03.006.

Miller, K. L., D. G. Torr, and P. G. Richards (1986), Meridional winds in the thermosphere derived from measurement of F_2 layer height, *J. Geophys. Res.*, *91*(A4), 4531–4535.

Oyama, K., S. Watanabe, Y. Su, T. Takahashi, and K. Hirao (1996), Season, local time, and longitude variations of electron temperature at the height of ~600 km in the low latitude region, *Adv. Space Res.*, *18*(6), 269–278, doi:10.1016/0273-1177(95)00936-1.

Rishbeth, H. (1967), The effect of winds on the ionospheric *F*2-peak, *J. Atmos. Terr. Phys.*, *29*(3), 225–238, doi:10.1016/0021-9169(67)90192-4.

Scherliess, L., and B. G. Fejer (1999), Radar and satellite global equatorial *F* region vertical drift model, *J. Geophys. Res.*, *104*(A4), 6829–6842.

Stoneback, R. A., R. A. Heelis, A. G. Burrell, W. R. Coley, B. G. Fejer, and E. Pacheco (2011), Observations of quiet time vertical ion drift in the equatorial ionosphere during the solar minimum period of 2009, *J. Geophys. Res.*, *116*, A12327, doi:10.1029/2011JA016712.

Sultan, P. J., and F. J. Rich (2001), Determination of a proxy for *F* region meridional neutral winds using in situ satellite ion density measurements, *J. Geophys. Res.*, *106*(A10), 21,033–21,038.

Venkatraman, S., and R. Heelis (2000), Interhemispheric plasma flows in the equatorial topside ionosphere, *J. Geophys. Res.*, *105*(A8), 18,457–18,464.

West, K. H., R. A. Heelis, and F. J. Rich (1997), Solar activity variations in the composition of the low-latitude topside ionosphere, *J. Geophys. Res.*, *102*(A1), 295–305, doi:10.1029/96JA03031.

Yue, X., W. Schreiner, J. Lei, S. Sokolovskiy, C. Rocken, D. Hunt, and Y. Kuo (2010), Error analysis of Abel retrieved electron density profiles from radio occultation measurements, *Ann. Geophys.*, *28*(1), 217–222.